Journal of Power Sources 266 (2014) 488–495

Contents lists available at ScienceDirect

Journal of Power Sources

journal homepage: www.elsevier.com/locate/jpowsour

Flexible all-solid-state supercapacitors based on graphene/carbon black nanoparticle film electrodes and cross-linked poly(vinyl alcohol)–H_2SO_4 porous gel electrolytes

Haojie Fei [1], Chongyang Yang [1], Hua Bao*, Gengchao Wang*

Shanghai Key Laboratory of Advanced Polymeric Materials, Key Laboratory for Ultrafine Materials of Ministry of Education, School of Materials Science and Engineering, East China University of Science and Technology, Shanghai 200237, PR China

HIGHLIGHTS

- A method is proposed to prepare cross-linked PVA–H_2SO_4 porous gel electrolyte.
- PVA porous membranes possess higher swelling ratio to H_2SO_4 aqueous solution.
- Graphene/CB films exhibit improved specific capacitance compared to graphene film.
- A flexible SC based on PVA porous gel electrolyte shows good performance at 70 °C.

GRAPHICAL ABSTRACT

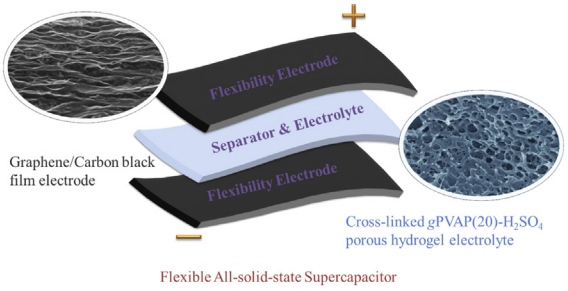

ARTICLE INFO

Article history:
Received 1 February 2014
Received in revised form
7 May 2014
Accepted 8 May 2014
Available online 21 May 2014

Keywords:
Poly(vinyl alcohol)
Porous gel electrolytes
Graphene
All-solid-state
Flexible supercapacitors

ABSTRACT

Flexible all-solid-state supercapacitors (SCs) are fabricated using graphene/carbon black nanoparticle (GCB) film electrodes and cross-linked poly(vinyl alcohol)–H_2SO_4 porous gel electrolytes (*g*PVAP–H_2SO_4). The GCB composite films, with carbon black (CB) nanoparticles uniformly distributed in the graphene nanosheets, greatly improve the active surface areas and ion transportation of pristine graphene film. The porous structure of as-prepared *g*PVAP–H_2SO_4 membrane improves the equilibrium swelling ratio in electrolyte and provides interconnected ion transport channels. The chemical cross-linking solves the fluidity problem of PVA–H_2SO_4 gel electrolyte at high temperature. As-fabricated GCB//*g*PVAP(20)–H_2SO_4//GCB flexible SC displays an increased specific capacitance (144.5 F g^{-1} at 0.5 A g^{-1}) and a higher specific capacitance retention (67.9% from 0.2 to 4 A g^{-1}). More importantly, the flexible SC possesses good electrochemical performance at high temperature (capacitance retention of 78.3% after 1000 cycles at 70 °C).

1. Introduction

Flexible energy storage devices that can function under considerable physical deformation have captured a great deal of attention for a wide range of applications such as wearable electronics, electronic newspapers and paper-like mobile phones [1–4]. The flexible supercapacitors (SCs) using gel polymer electrolytes (GPEs) and flexible electrode materials [5,6] have been recognized as promising portable energy storage devices due to their high

* Corresponding authors. Tel.: +86 21 64253527; fax: +86 21 64251372.
E-mail addresses: baohua@ecust.edu.cn (H. Bao), gengchaow@ecust.edu.cn (G. Wang).
[1] These authors contributed equally to this work.

http://dx.doi.org/10.1016/j.jpowsour.2014.05.059
0378-7753/

power density and long cycle lifetime compared with lithium-ion batteries [7–11].

The gel polymer electrolytes exhibit higher conductivity than solvent-free solid electrolytes and are effective at retaining liquid to prevent evaporation and leakage [6,8,12], holding the key to practical applications in flexible SCs. More recently, intensive efforts have been devoted to various gel polymer electrolyte systems for flexible SCs, such as PVA-acid or alkali [9–16], polyethylene oxide (PEO)-alkali [13,17,18], potassium polyacrylate (PAAK)-salt or alkali [19–21], polyacrylamide (PAAM)-acid or alkali [22,23]. Among them, PVA is considered to be a prospective GPE due to its easy preparation, excellent hydrophilicity, good film-forming and chemical-resistant properties [24,25]. PVA–H_2SO_4, usually fabricated by a solvent casting method, is the most commonly used acid hydrogel electrolyte in flexible SCs [8,26,27]. However, PVA–H_2SO_4 presents some fluidity under higher temperature, which greatly limits its high-temperature applications.

PVA hydrogel electrolytes with cross-linked polymer networks exhibit a high liquid uptake while maintaining the dimensional stability of a solid system, which is appropriate to flexible SCs at high temperature and substitute for weak gel electrolytes [28]. So far, the modification of PVA hydrogel electrolytes was concentrated mainly upon enhancing their performance using polyacrylic acid (PAA) [29], poly(2-acrylamido-2-methyl-1-propanesulfonic) acid (PAMPS) [30], poly(vinyl chloride) (PVC) [31], poly(2-hydroxyethyl methacrylate) (PHEMA) [32], poly(vinyl pyrrolidone) (PVP) [33], polystyrene sulfonic acid (PSSA) [34] and crosslink agent like glutaraldehyde (GA) and poly(ethylene glycol) diglycidyl ether (PEGDGE) [35]. Most of them were applied as proton-exchange membranes for direct methanol fuel cells. However, to our knowledge, there have been no reports on flexible SCs based on the modified PVA hydrogel electrolytes so far.

Graphene, a 2D layer of sp^2-bonded carbon, exhibits strong mechanical strength, high electrical conductivity, large surface area and superior flexibility, which is a promising material for flexible electrodes [36–39]. However, as-prepared individual graphene nanosheets are tending to restack together during the fabrication of electrodes due to the strong van der Waals interactions, decreasing the specific capacitance and specific surface areas for energy storage [40,41]. Great efforts have been devoted to decrease the restacking [37,42–44]. Among them, one method is to use carbon nanotubes (CNTs) to intercalate into the graphene nanosheets, bridging the defects for electron transfer and increasing the basal spacing between graphene sheets [45–48]. However, carbon black pillared graphene sheets composite films were rarely reported [49].

Herein, we fabricate a novel flexible all-solid-state supercapacitor (SC) based on cross-linked poly(vinyl alcohol)–H_2SO_4 porous gel electrolyte (*g*PVAP–H_2SO_4) and graphene/carbon black nanoparticle (GCB) composite films as flexible electrodes. *g*PVAP–H_2SO_4 membranes are modified by poly(vinyl pyrrolidone) (PVP) as pore-forming agent to enhance their swelling ratio in H_2SO_4 electrolyte and are cross-linked using glutaraldehyde (GA) as cross-linking agent to solve the fluidity and thermal aging problems of PVA under high temperature. The GCB composite films are prepared by a vacuum-infiltration method. As-fabricated SC device based on *g*PVAP–H_2SO_4 gel electrolyte shows excellent electrochemical performance at 70 °C compared with traditional PVA–H_2SO_4 system.

2. Experimental

2.1. Preparation of cross-linked PVA–H_2SO_4 porous electrolyte membranes

PVP (K30, M_w = 58,000) and PVA (99% hydrolyzed, average polymerization degree is 1750 ± 50) aqueous solutions were prepared by dissolving 2 g powders (total mass) in 24 mL deionized water and heating at 90 °C under agitation. The weight ratios of PVP and PVA were 0/100, 10/90, 20/80, and 30/70. GA cross-linking agent (1.25 wt% of PVA) and 200 μL of 2 M H_2SO_4 catalyst were added after the polymer solutions were cooled to the room temperature. The mixed solutions were stirred for 20 min and then degassed. The resultant solutions were cast onto glass plates, cured at 35 °C for 6 h and dried at 50 °C to form cross-linked PVA/PVP composite membranes. The PVA/PVP composite membranes were immersed in excess of deionized water to remove PVP from PVA matrix to form porous structure, followed by freeze drying. The obtained cross-linked PVA porous membranes were labeled as *g*PVA, *g*PVAP(10), *g*PVAP(20) and *g*PVAP(30), respectively. The as-prepared *g*PVAP membranes were soaked in 1 M H_2SO_4 for 5 days to obtain *g*PVAP–H_2SO_4 electrolyte membranes.

2.2. Preparation of graphene/carbon black nanoparticle flexible electrodes

Graphene colloidal solution was prepared by an electrostatic stabilization method [50]. Typical procedure was as follows: graphite oxide (GO) was synthesized from graphite powder using the Hummers method [51]. The as-prepared graphite oxide was exfoliated in pH = 10 ammonia solution under intermittent ultrasonication for 40 min, centrifuged at 3000 rpm to remove the aggregations and then diluted to 2.5 mg mL^{-1}. The resultant GO colloidal solution (7 mL) was mixed with hydrazine hydrate (80 wt %, 40 μL), ammonia solution (25–28 wt%, 0.45 mL) and deionized water (120 mL), and then vigorously stirred for 30 min. The well-mixed solution was maintained at 97 °C without stirring for 1 h.

2 mg carbon black nanoparticles [Super P®, specific surface area (BET): 62 m^2 g^{-1}, diameter: ~40 nm], treated with nitric acid [52], were dispersed in deionized water (20 mL) followed by ultrasonication for 2 h. Graphene colloidal solution was mixed with the as-prepared carbon black nanoparticle dispersion and sonicated for 15 min. The graphene/carbon black nanoparticle (GCB) composite films were prepared by filtrating GCB dispersions through the polyvinylidene fluoride (PVDF) filter membranes (0.45 μm pore size), followed by washing, air drying, and peeling off from the filter membranes. The as-prepared GCB films were transferred onto polyethylene terephthalate (PET) substrates and then cut into pieces of 1 cm × 2 cm. Thin silver glue was coated on the edge of each film for electrical contact. As a compared sample, graphene film was prepared by the similar procedure above without the presence of carbon black nanoparticles.

2.3. Fabrication of flexible all-solid-state SC devices

Prior to fabricating SC devices, two pieces of GCB composite film were immersed in 1 M H_2SO_4 aqueous solution with 1 wt% PVA for 12 h at room temperature to ensure that the electrolyte completely wets the electrodes. The flexible all-solid-state SC was prepared with a *g*PVAP(20)–H_2SO_4 electrolyte membrane sandwiched by two symmetric GCB flexible electrodes under pressing. For comparison, the graphene//*g*PVAP(20)–H_2SO_4//graphene flexible all-solid-state SC was prepared through the similar protocol above.

In order to integrate GCB//PVA–H_2SO_4//GCB flexible SC, PVA–H_2SO_4 solution was prepared with the following procedure. 10 g of H_2SO_4 was mixed with 100 mL of deionized water, and then 10 g of PVA powder was added. The whole mixture was heated to 85 °C under stirring until the solution became clear. Two pieces of GCB film were immersed in the PVA–H_2SO_4 solution for 12 h with the silver glue part out of the solution. Subsequently, the films were left under ambient conditions for 5 h to vaporize the excess water. Then the two film electrodes were pressed together to obtain

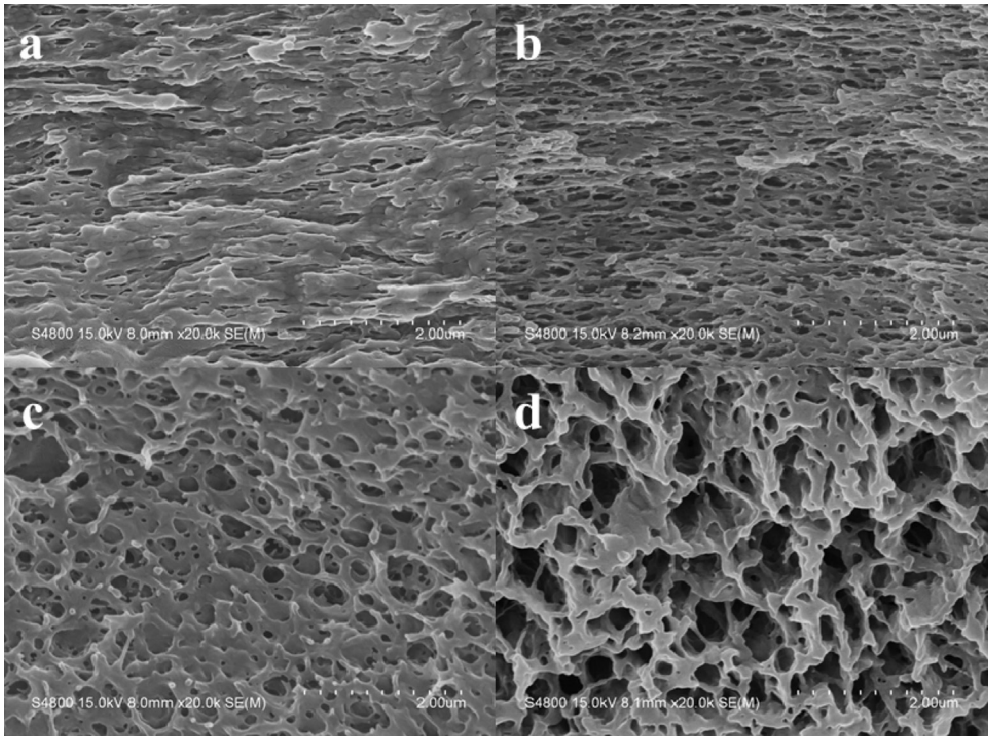

Fig. 1. Cross-sectional FE-SEM images of hydrogel polymer membranes: (a) *g*PVA, (b) *g*PVAP(10), (c) *g*PVAP(20), (d) *g*PVAP(30).

flexible SC device. PVA–H_2SO_4 gel electrolyte membrane was prepared by leaving the PVA–H_2SO_4 solution under ambient conditions for 5 h.

2.4. Characterizations

The morphologies of as-prepared samples were observed by field-emission scanning electron microscope (FE-SEM, Hitachi S-4800). The specific surface areas (SSA) of flexible electrode materials were tested on Molecular Devices SpectraMax M2 using the methylene blue adsorption technique (the measurement details are provided in Supplementary information).

The equilibrium swelling ratio (ESR) can be estimated using the following equation: $\mathrm{ESR}(\%) = (W_t - W_d) \times 100/W_d$, where W_d is the dry weight of membranes dried in a vacuum oven at 50 °C, W_t is the wet weight of membranes after reaching the swelling equilibrium in 1 M H_2SO_4.

Tensile strength of *g*PVAP–H_2SO_4 electrolyte membranes (20 mm × 50 mm) at swelling equilibrium condition was measured on a Zwick Roell testing system at room temperature. The length between the jaws was 30 mm, and the tensile speed was 100 mm min^{-1}.

2.5. Electrochemical measurement of the flexible SCs devices

Electrochemical performance was performed by cyclic voltammetry (CV), galvanostatic charge/discharge tests and electrochemical impedance spectroscopy (EIS) on a CHI 660D electrochemical workstation. And the cycling stability was conducted on a LAND CT2001A program testing system. All of the experiments were carried out in a two-electrode configuration. The specific capacitance (C_s) of the electrode materials could be calculated from galvanostatic charge/discharge curves according to following equation: $C_s = 2It/(m\Delta V)$, where I is the discharge current, t is the discharge time, m is the mass of active electrode materials on single electrode and ΔV is the voltage change upon discharging after *IR* drop.

3. Results and discussion

To study the microstructures and morphologies of cross-linked PVA porous membranes, FE-SEM analysis is employed. Pores could hardly be found in *g*PVA membrane (Fig. 1a). However, the microstructures of *g*PVAP membranes significantly changed after being modified with PVP. The *g*PVAP membranes show highly and uniformly interconnected porous structures, which result from the removal of PVP pore-forming agent after being immersed in excess of deionized water. It is found that the pore size increases upon the

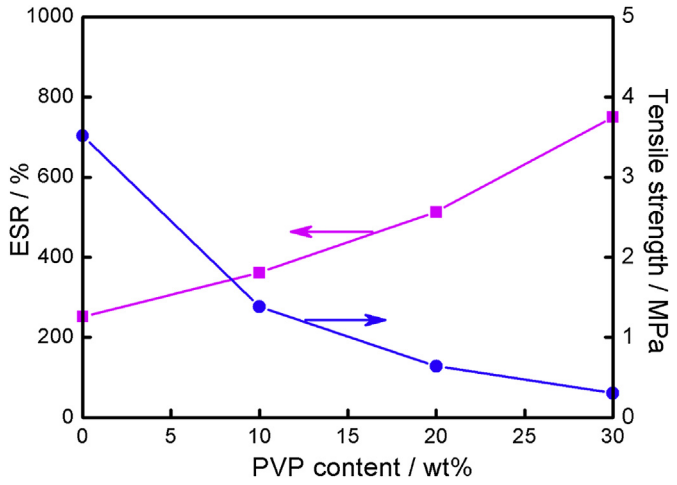

Fig. 2. Influence of PVP content on swelling ratio and tensile strength of *g*PVAP–H_2SO_4 hydrogel electrolyte membranes.

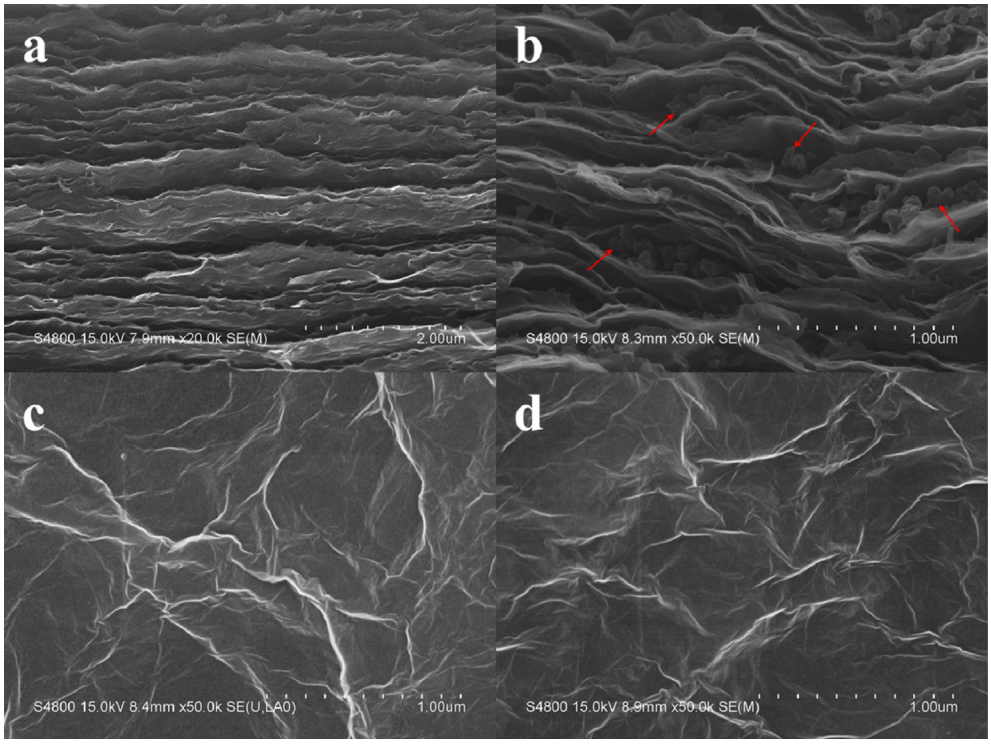

Fig. 3. Cross-sectional FE-SEM images of (a) graphene film and (c) GCB composite film. Superficial FE-SEM images of (b) graphene film and (d) GCB composite film.

addition of PVP. The pore diameter of *g*PVAP(10) membrane is in the range of 100–400 nm (Fig. 1b). When the amount of PVP is increased to 20 wt% and 30 wt%, *g*PVAP membranes show well interconnected pores with the pore diameter of 100 nm to 1 μm (Fig. 1c and d).

As shown in Fig. 2, the influence of PVP content on equilibrium swelling ratio (ESR) and tensile strength of *g*PVAP–H_2SO_4 gel electrolyte membranes is significant. With increasing PVP content, the ESR increases and the tensile strength decreases. When the content of PVP is 20 wt%, the ESR and tensile strength are 513.5% and 0.64 MPa, respectively. The well interconnected porous structure could accommodate large amount of electrolyte, which contributes to a high ESR. Besides, the ionic conductivity is closely related with ESR. When the PVP content changes from 0 to 20 wt%, the ionic conductivity significantly increases. Further increasing the PVP content to 30 wt% results in no obvious improvement of ionic conductivity (Fig. S1). The ionic conductivities of *g*PVAP(20)–H_2SO_4 and PVA–H_2SO_4 gel electrolyte membranes at 20 °C are 24.9×10^{-3} and 24.1×10^{-3} S cm^{-1}, respectively. It is also found that the ionic conductivities of *g*PVAP(20)–H_2SO_4 and PVA–H_2SO_4 gel electrolyte membranes increase over the range of 10–70 °C (Fig. S2). Besides, to avoid short circuit of two electrodes especially under the bent and twisted state, high mechanical strength of gel electrolyte is quite essential for flexible devices. And the tensile strength of *g*PVAP(20)–H_2SO_4 gel electrolyte membrane is twice that of *g*PVAP(30)–H_2SO_4 gel electrolyte membrane. Therefore, on the basis of the ESR, ionic conductivity and mechanical strength, *g*PVAP(20)–H_2SO_4 is chosen as gel electrolyte for the assembly of flexible all-solid-state SC devices.

The cross-sectional and superficial morphologies of graphene and GCB flexible films are characterized by FE-SEM, as shown in Fig. 3. The highly oriented layered structure is observed from the cross-section images (Fig. 3a and b). The individual graphene nanosheets can easily restack into compact layered structure (Fig. 3a) when forming free-standing film electrodes, which is difficult for electrolyte ions to access the surface of graphene. In the GCB composite film, CB nanoparticles are uniformly distributed in the graphene nanosheets as effective spacers to restrain the restacking and aggregation of graphene nanosheets (Fig. 3b). In addition, GCB composite film displays an unsmooth and crumpled surface similar to graphene film (Fig. 3c and d), indicating the introduction of CB nanoparticles does not apparently change the superficial morphologies of graphene.

The configuration of flexible all-solid-state SCs described herein is schematically shown in Fig. 4. The GCB//*g*PVAP(20)–H_2SO_4//GCB flexible SC is assembled using two symmetric GCB film electrodes separated with a *g*PVAP(20)–H_2SO_4 membrane (Fig. 4a). The *g*PVAP(20)–H_2SO_4 membrane is transparent, and is used as both electrolyte and separator (Fig. 4b). Two GCB films simultaneously serve as electrodes and current collectors (Fig. 4c). Fig. 4d exhibits the appearances of as-fabricated SC device under regular and bending situation. The as-fabricated SC is highly flexible and can be bended without destroying the structural integrity of the device. For comparison, graphene//*g*PVAP(20)–H_2SO_4//graphene and GCB//PVA–H_2SO_4//GCB flexible SCs are also fabricated.

The incorporation of CB nanoparticles into graphene nanosheets has significant influence on the specific surface area (SSA) and specific capacitance of GCB flexible films. As shown in Fig. 5, the SSA gradually increases with increasing CB content and reaches the maximum (744 m^2 g^{-1}) with the CB content of 2 mg. It is mainly due to that the introduction of CB nanoparticles prevents the agglomeration and stacking of graphene nanosheets and expands the layer distance between graphene nanosheets. However, when further increasing the CB content to 3 mg, the SSA goes down instead. This can be ascribed to that CB nanoparticles have lower specific surface area than graphene, leading to the decreasing trend of SSA. Interestingly, it is found that the variation trend of specific capacitance relative to CB content is similar to the SSA, which may be due to that the specific capacitance for GCB composite films is closely associated with their SSA. The maximum specific

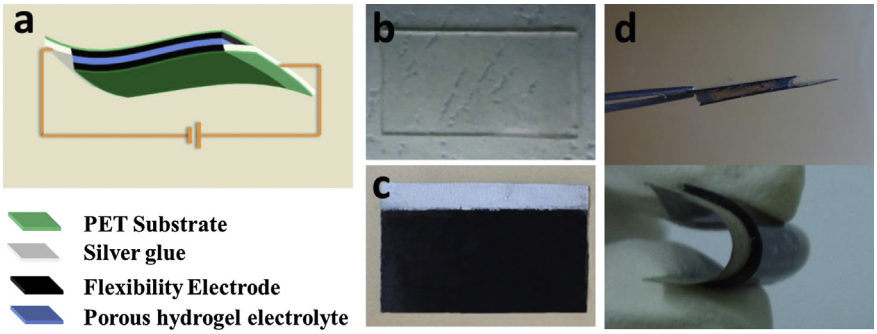

Fig. 4. (a) Schematic diagram of flexible supercapacitor. Photographs of (b) gPVAP(20)–H_2SO_4 electrolyte membrane, (c) GCB flexible electrode with silver glue, (d) flexible supercapacitor under regular and bending situation.

capacitance of 144.5 F g^{-1} is obtained with the CB content of 2 mg. Hence, the optimal weight of CB in GCB flexible film is 2 mg.

In order to further validate the influence of CB nanoparticles on graphene flexible electrodes, the electrochemical performance of graphene//gPVAP(20)–H_2SO_4//graphene and GCB//gPVAP(20)–H_2SO_4//GCB flexible SCs is analyzed by cycle voltammetry (CV), galvanostatic charge–discharge and electrochemical impedance spectroscopy (EIS). Both CV curves of graphene and GCB exhibit relatively regular rectangular shapes at the scan rate of 10 mV s^{-1} (Fig. 6a). And the charge–discharge curves of graphene and GCB are linear, symmetric and triangular (Fig. 6b), reflecting the typical reversible capacitive characteristics of electric double-layer capacitors. However, when comparing the CV curves of graphene and GCB SCs, the GCB SC displays more rectangular-shaped profile and larger integral area. The specific capacitance (C_s) of GCB calculated from charge/discharge curves is 144.5 F g^{-1} at the current density of 0.5 A g^{-1}, higher than that of graphene (107.5 F g^{-1}). This is attributed to the fact that CB nanoparticles behave as the pillars between the interlayer of graphene nanosheets and GCB provides larger SSA (744 m^2 g^{-1}) than graphene (640 m^2 g^{-1}). Impressively, compared with graphene, GCB not only exhibits higher specific capacitance but also retains better rate capacity (Fig. 6c) with specific capacitance retention of 67.9% (0.2 A g^{-1} to 4 A g^{-1}), superior to graphene (63.2% from 0.2 A g^{-1} to 3 A g^{-1}).

EIS is a powerful tool to understand the fundamental behaviors of electrode materials. As demonstrated in Fig. 6d, Nyquist plots show a straight line at the low frequency region and a semicircle at the high frequency region. The straight line which is nearly parallel to the imaginary axis reflects the ideal capacitive behavior of the devices. At high frequency, the intercept on the real axis represents the ohmic resistance (R_s). The semicircle corresponds to the charge transfer resistance (R_{ct}) at the electrode/electrolyte interface, which is strongly dependent on the abilities of ion transfer and electron conduction [53,54]. It can be seen that the R_s (17.1 Ω) and R_{ct} (3.3 Ω) of GCB are obviously lower than those of graphene (22.0 and 14.4 Ω). This result demonstrates that CB nanoparticles not only act as a conductive bridge by connecting the neighboring layers of graphene, but also prevent the self-restacking of graphene nanosheets to facilitate the diffusion of electrolyte ions into the interior of the electrodes. It is apparent that the SCs with GCB have excellent advantage over that without CB.

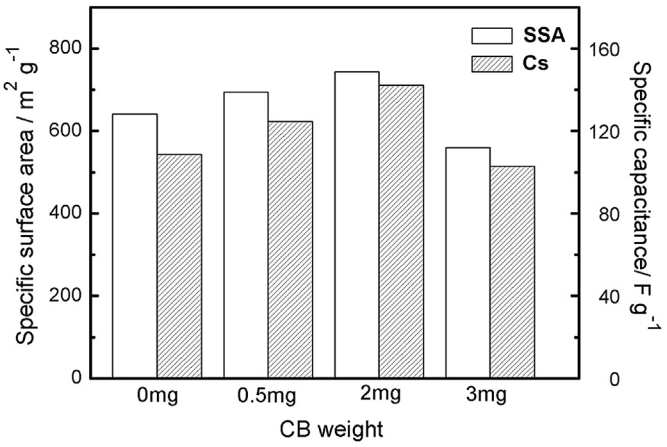

Fig. 5. Influence of CB content on the specific capacitance and the specific surface area of GCB film.

Simultaneously, gPVAP(20)–H_2SO_4 is suggested to be capable as a gel electrolyte, which is also confirmed in our research for its similar CV curve compared with PVA–H_2SO_4 gel electrolyte at room temperature (Fig. S3). To further confirm the superiorities of gPVAP(20)–H_2SO_4 for flexible SCs, the electrochemical performance of flexible SCs is carried out at elevated temperature. Fig. 7a shows charge–discharge curves of GCB//gPVAP(20)–H_2SO_4//GCB flexible SC at 0.5 A g^{-1} under various temperatures. It can be seen that the charge/discharge curve of flexible SC displays a good linear and symmetric relation in a range of 20–80 °C, revealing that the as-fabricated flexible SC device functions well in a wide temperature range. The specific capacitance (C_s) calculated from discharging curves increases from 144.5 to 183.1 F g^{-1} along with the rise of temperature from 20 to 80 °C. Since the capacitance depends upon the amount of ions at the vicinity of electric double layer, the improvement of C_s can be ascribed to that the diffusion of ions into micropores between graphene nanosheets is significantly enhanced with increasing temperature [55].

Adaptability of as-fabricated flexible SCs for high-temperature applications is demonstrated by comparing the cycling durability at room temperature and 70 °C, as shown in Fig. 7b. At room temperature, the flexible SC device assembled with gPVAP(20)–H_2SO_4 gel electrolyte displays 89.0% retention of the initial capacitance after 1000 charge–discharge cycles, which is comparable with that obtained with PVA–H_2SO_4 gel electrolyte. The specific capacitance of the SC with gPVAP(20)–H_2SO_4 decreases apparently in the initial 200 cycles and maintains steady in the following cycles with the capacitance retention of 78.3% (1000 cycles) at a high testing temperature of 70 °C. However, due to the fluidity of PVA–H_2SO_4 gel electrolyte at high temperature (70 °C), the cycle stability of its SC is not able to be tested. These results indicate that flexible SC fabricated with gPVAP(20)–H_2SO_4 possesses superior electrochemical stability at high temperature, which can meet the needs of high-temperature energy storage.

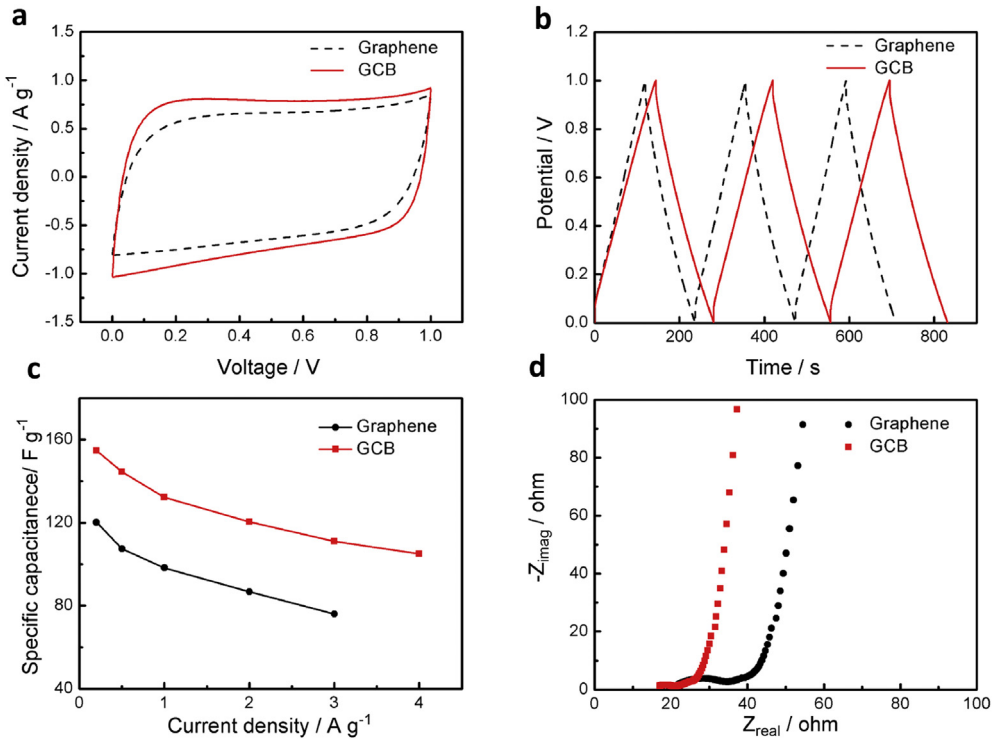

Fig. 6. Electrochemical performance of graphene//*g*PVAP(20)–H_2SO_4//graphene and GCB//*g*PVAP(20)–H_2SO_4//GCB flexible supercapacitors. (a) Cyclic voltammograms at a scan rate of 10 mV s^{-1}. (b) Galvanostatic charge/discharge curves at a current density of 0.5 A g^{-1}. (c) Specific capacitances at different current densities. (d) Nyquist plots.

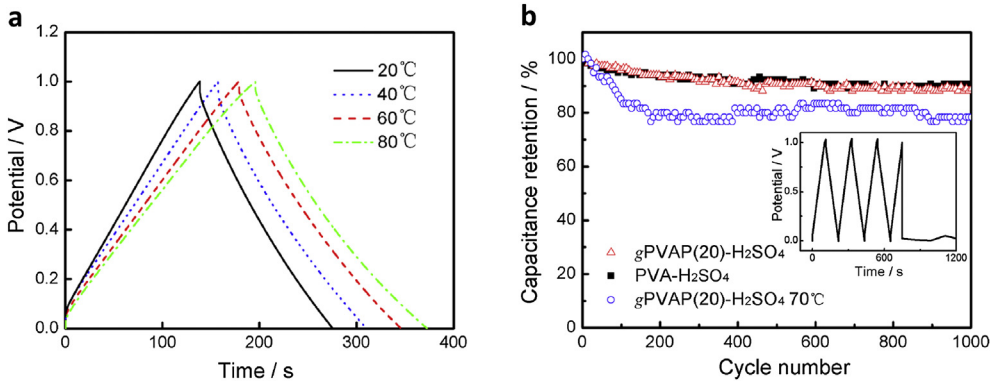

Fig. 7. (a) Charge–discharge curves of GCB//*g*PVAP(20)–H_2SO_4//GCB flexible supercapacitor under various temperatures. (b) Cycling stability of GCB//*g*PVAP(20)–H_2SO_4//GCB and GCB//PVA–H_2SO_4//GCB flexible supercapacitors at room temperature and 70 °C. The inset shows the galvanostatic charge/discharge curve for GCB//PVA–H_2SO_4//GCB flexible supercapacitor at 70 °C.

The thermal stability of polymer gel electrolyte membrane is a key factor for high-temperature use. Fig. 8 presents the changes of the appearance for *g*PVAP(20)–H_2SO_4 and PVA–H_2SO_4 gel electrolyte membranes before and after thermal treatment at 70 °C for 5 h. Interestingly, *g*PVAP(20)–H_2SO_4 gel electrolyte membrane is still colorless and transparent after thermal treatment while PVA–H_2SO_4 gel electrolyte membrane turns yellow. It can be explained by the fact that cross-linked network structure maintains the dimensional stability, which ensures that the low concentration of H_2SO_4 can be accommodated in gel electrolyte membrane. As a result, thermal damage of *g*PVAP(20)–H_2SO_4 gel electrolyte membrane could hardly be observed. In comparison, the PVA–H_2SO_4 gel electrolyte membrane was prepared by evaporating the excess water of PVA–H_2SO_4 solution in order to decrease the fluidity of PVA–H_2SO_4 solution. As a result, the concentration of H_2SO_4 in gel electrolyte membrane becomes very high, leading to the degradation and oxidation of PVA membrane. Thus the above results further demonstrate that *g*PVAP(20)–H_2SO_4 gel electrolyte membrane possesses excellent thermal aging resistance.

In order to evaluate the potential of the as-fabricated SC with *g*PVAP(20)–H_2SO_4 membrane and GCB composite films for flexible energy storage devices, the electrochemical performance of the all-solid-state SC is measured under bending conditions at different bending angles. Interestingly, the change of CV curves of as-fabricated SC seems to be tiny and acceptable when the bending angle changes from 0 to 120° (Fig. 9a), revealing that the bending has nearly no effect on the capacitive performance.

The durability performance of GCB//*g*PVAP(20)–H_2SO_4//GCB SC under cyclic strains should be addressed to demonstrate the potential for flexible energy-storage devices. The durability

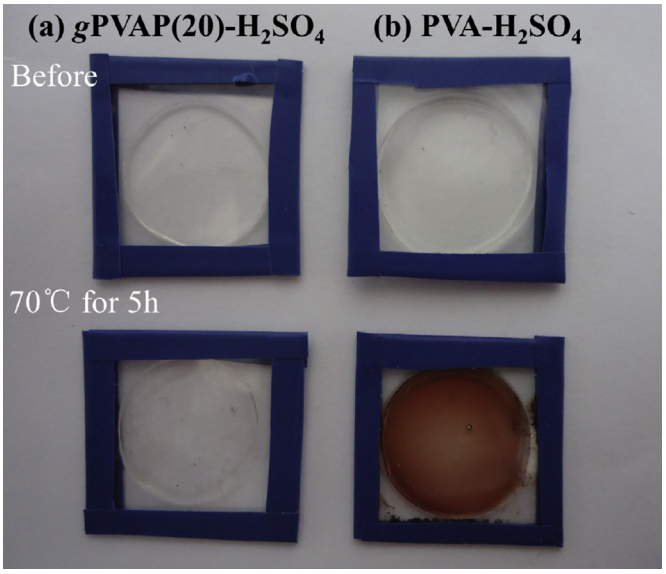

Fig. 8. The digital photo of different polymer gel electrolyte membranes before and after thermal treatment at 70 °C for 5 h. (a) gPVAP(20)–H_2SO_4, (b) PVA–H_2SO_4.

performance is evaluated by galvanostatic charge–discharge tests after the SC is bended back and forth at an angle of 60° for 300 cycles, as shown in Fig. 9b. The main loss of specific capacitance occurs in the initial 100 cycles (84.9% remained) and only a little fading can be observed in the following cycles. And the capacitance retention is 80.2% after 300 cycles. This superior performance is ascribed to the excellent mechanical robustness, intimate interfacial contact among the multiple components, and the electrical conductivity of the devices.

Due to the narrow voltage window of hydrogel electrolyte, device packs with two or more devices connected in series need to be assembled in order to meet the higher voltages of portable equipment. Adding electrochemical capacitors together in a serial string increases the voltage, while the current remains the same. Here, the performance of electrochemical capacitor packs with three flexible devices connected in series is measured. As can be seen, at the same charge/discharge current, the voltage is extended from 1 V for a single device to 3 V for a cell pack (Fig. 10a). This charged electrochemical capacitor pack can light up a red light-emitting-diode (LED), demonstrating the application prospect for as-fabricated flexible SC (Fig. 10b).

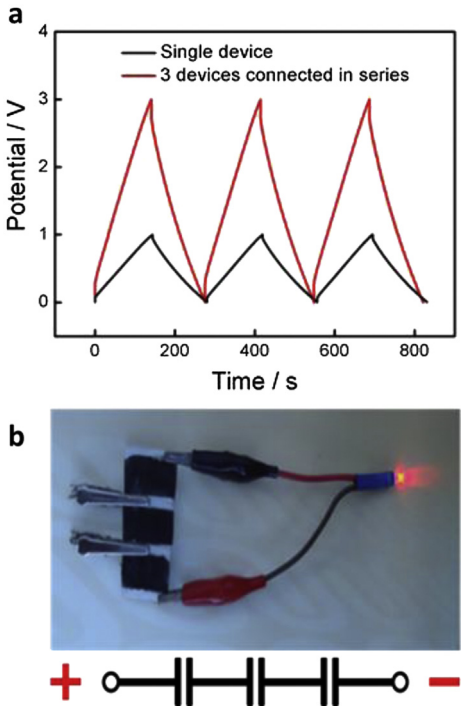

Fig. 10. (a) Charge–discharge curves at 0.5 A g^{-1} of single GCB//gPVAP(20)–H_2SO_4//GCB supercapacitor and three supercapacitors in series. (b) Photograph of a red LED lighted by three flexible supercapacitors in series. (For interpretation of the references to color in this figure legend, the reader is referred to the web version of this article.)

4. Conclusions

We have successfully developed a novel flexible all-solid-state SC configuration with two separated GCB film electrodes and cross-linked poly(vinyl alcohol)–H_2SO_4 porous gel electrolyte (gPVAP–H_2SO_4). The as-assembled GCB//gPVAP(20)–H_2SO_4//GCB flexible SC exhibits an increased specific capacitance of 144.5 F g^{-1} at a current density of 0.5 A g^{-1} and better rate capability (67.9% capacitance retention as current density increases from 0.2 to 4 A g^{-1}). Meanwhile, the flexible SC still remains a nearly invariant electrochemical performance under highly bent (testing) condition. More importantly, our SC device possesses excellent cycling stability with 78.3% retention of the initial specific capacitance after 1000 cycles at a high temperature of 70 °C. The unique structure

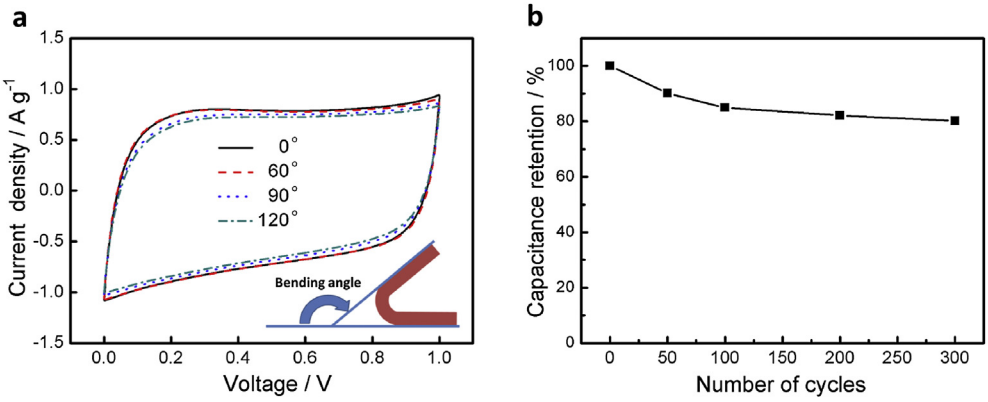

Fig. 9. Durability performance test GCB//gPVAP(20)–H_2SO_4//GCB flexible supercapacitor. (a) Cyclic voltammograms at various bending angles. (b) Capacitance retention after various bending cycles at angle of 60°.

and the positive synergistic effects of flexible electrode material and cross-linked porous gel electrolyte contribute to the improved performances. These superior electrochemical performances indicate that the flexible all-solid-state SC described in this work may offer great promise in the application of high-temperature energy storage systems.

Acknowledgments

We greatly appreciate the financial supports of National Natural Science Foundation of China (51173042), Fundamental Research Funds for the Central Universities, Shanghai Municipal Science and Technology Commission (12nm0504102).

Appendix A. Supplementary data

Supplementary data related to this article can be found at http://dx.doi.org/10.1016/j.jpowsour.2014.05.059.

References

[1] J.R. Miller, Science 335 (2012) 1312–1313.
[2] F. Liu, S.Y. Song, D.F. Xue, H.J. Zhang, Adv. Mater. 24 (2012) 1089–1094.
[3] L. Nyholm, G. Nyström, A. Mihranyan, M. Strømme, Adv. Mater. 23 (2011) 3751–3769.
[4] H. Gwon, H.S. Kim, K.U. Lee, D.H. Seo, Y.C. Park, Y.S. Lee, B.T. Ahn, K. Kang, Energy Environ. Sci. 4 (2011) 1277–1283.
[5] C.L. Lai, Z.P. Zhou, L.F. Zhang, X.X. Wang, Q.X. Zhou, Y. Zhao, Y.C. Wang, X.F. Wu, Z.T. Zhu, H. Fong, J. Power Sources 247 (2014) 134–141.
[6] M. Kaempgen, C.K. Chan, J. Ma, Y. Cui, G. Gruner, Nano Lett. 9 (2009) 1872–1876.
[7] Y.J. Kang, S.J. Chun, S.S. Lee, B.Y. Kim, J.H. Kim, H. Chung, S.Y. Lee, W. Kim, ACS Nano 6 (2012) 6400–6406.
[8] P.J. Hall, M. Mirzaeian, S.I. Fletcher, F.B. Sillars, A.J.R. Rennie, G.O. Shitta-Bey, G. Wilson, A. Cruden, R. Carter, Energy Environ. Sci. 3 (2010) 1238–1251.
[9] C.Z. Meng, C.H. Liu, L.Z. Chen, C.H. Hu, S.S. Fan, Nano Lett. 10 (2010) 4025–4031.
[10] L.Y. Yuan, X.H. Lu, X. Xiao, T. Zhai, J.J. Dai, F.C. Zhang, B. Hu, X. Wang, L. Gong, J. Chen, C.G. Hu, Y.X. Tong, J. Zhou, Z.L. Wang, ACS Nano 6 (2012) 656–661.
[11] B.G. Choi, J. Hong, W.H. Hong, P.T. Hammond, H. Park, ACS Nano 5 (2011) 7205–7213.
[12] F.H. Meng, Y. Ding, Adv. Mater. 23 (2011) 4098–4102.
[13] N.A. Choudhury, S. Sampath, A.K. Shukla, Energy Environ. Sci. 2 (2009) 55–67.
[14] H. Wada, K. Yoshikawa, S. Nohara, N. Furukawa, H. Inoue, N. Sugoh, H. Iwasaki, C. Iwakura, J. Power Sources 159 (2006) 1464–1467.
[15] H. Gao, H. Wu, K. Lian, Electrochem. Commun. 17 (2012) 48–51.
[16] X.H. Lu, G.M. Wang, T. Zhai, M.H. Yu, S.L. Xie, Y.C. Ling, C.L. Liang, Y.X. Tong, Y. Li, Nano Lett. 12 (2012) 5376–5381.
[17] D. Kalpana, N.G. Renganathan, S. Pitchumani, J. Power Sources 157 (2006) 621–623.
[18] A. Lewandowski, M. Zajder, E. Frackowiak, F. Beguin, Electrochim. Acta 46 (2001) 2777–2780.
[19] H.S. Nam, N.L. Wu, K.T. Lee, K.M. Kim, C.G. Yeom, L.R. Hepowit, J.M. Ko, J.D. Kim, J. Electrochem. Soc. 159 (2012) A899–A903.
[20] K.T. Lee, N.L. Wu, J. Power Sources 179 (2008) 430–434.
[21] S. Nohara, T. Asahina, H. Wada, N. Furukawa, H. Inoue, N. Sugoh, H. Iwasaki, C. Iwakur, J. Power Sources 157 (2006) 605–609.
[22] I. Stepniak, A. Ciszewski, Electrochim. Acta 56 (2011) 2477–2482.
[23] I. Stepniak, A. Ciszewski, Electrochim. Acta 54 (2009) 7396–7400.
[24] C.P. Liu, C.A. Dai, C.Y. Chao, S.J. Chang, J. Power Sources 249 (2014) 285–298.
[25] G.M. Wu, S.J. Lin, C.C. Yang, J. Power Sources 244 (2013) 287–293.
[26] B.G. Choi, S.J. Chang, H.W. Kang, C.P. Park, H.J. Kim, W.H. Hong, S.G. Lee, Y.S. Huh, Nanoscale 4 (2012) 4983–4988.
[27] Y.X. Xu, Z.Y. Lin, X.Q. Huang, Y. Liu, Y. Huang, X.F. Duan, ACS Nano 7 (2013) 4042–4049.
[28] H.C. Gao, F. Xiao, C.B. Ching, H.W. Duan, ACS Appl. Mater. Interfaces 4 (2012) 7020–7026.
[29] N.A. Choudhury, A.K. Shukla, S. Sampath, S. Pitchumani, J. Electrochem. Soc. 153 (2006) A614–A620.
[30] J.L. Qiao, T. Hamaya, T. Okada, Polymer 46 (2005) 10809–10816.
[31] C.C. Yang, G.M. Wu, Mater. Chem. Phys. 114 (2009) 948–955.
[32] J.M. Yang, C.Y. Chiang, H.Z. Wang, C.C. Yang, J. Membr. Sci. 341 (2009) 186–194.
[33] N. Rajeswari, S. Selvasekarapandian, S. Karthikeyan, M. Prabu, G. Hirankumar, H. Nithya, C. Sanjeeviraja, J. Non-Cryst. Solids 357 (2011) 3751–3756.
[34] A.K. Sahu, G. Selvarani, S. Pitchumani, P. Sridhar, A.K. Shukla, N. Narayanan, A. Banerjee, N. Chandrakumar, J. Electrochem. Soc. 155 (2008) B686–B695.
[35] G. Merle, S.S. Hosseiny, M. Wessling, K. Nijmeijer, J. Membr. Sci. 409–410 (2012) 191–199.
[36] L.M. Dai, Acc. Chem. Res. 46 (2013) 31–42.
[37] X.W. Yang, C. Cheng, Y.F. Wang, L. Qiu, D. Li, Science 341 (2013) 534–537.
[38] H.M. Jeong, J.W. Lee, W.H. Shin, Y.J. Choi, H.J. Shin, J.K. Kang, J.W. Choi, Nano Lett. 11 (2011) 2472–2477.
[39] Y.W. Zhu, S. Murali, M.D. Stoller, K.J. Ganesh, W.W. Cai, P.J. Ferreira, A. Pirkle, R.M. Wallace, K.A. Cychosz, M. Thommes, D. Su, E.A. Stach, R.S. Ruoff, Science 332 (2011) 1537–1541.
[40] C. Cheng, D. Li, Adv. Mater. 25 (2013) 13–30.
[41] K. Zhang, L.L. Zhang, X.S. Zhao, J.S. Wu, Chem. Mater. 22 (2010) 1392–1401.
[42] M.F. El-Kady, V. Strong, S. Dubin, R.B. Kaner, Science 335 (2012) 1326–1330.
[43] L. Qiu, X.H. Zhang, W.R. Yang, Y.F. Wang, G.P. Simon, D. Li, Chem. Commun. 47 (2011) 5810–5812.
[44] Z.Q. Niu, J. Chen, H.H. Hng, J. Ma, X.D. Chen, Adv. Mater. 24 (2012) 4144–4150.
[45] J. Li, X.Q. Cheng, A. Shashurin, M. Keidar, Graphene 1 (2012) 1–13.
[46] H.Y. Sun, Z. Xu, C. Gao, Adv. Mater. 25 (2013) 2554–2560.
[47] Y.Q. Sun, Q. Wu, G.Q. Shi, Energy Environ. Sci. 4 (2011) 1113–1132.
[48] Z.J. Fan, J. Yan, L.J. Zhi, Q. Zhang, T. Wei, J. Feng, M.L. Zhang, W.Z. Qian, F. Wei, Adv. Mater. 22 (2010) 3723–3728.
[49] G.K. Wang, X. Sun, F.Y. Lu, H.T. Sun, M.P. Yu, W.L. Jiang, C.S. Liu, J. Lian, Small 8 (2012) 452–459.
[50] D. Li, M.B. Müller, S. Gilje, R.B. Kaner, G.G. Wallace, Nat. Nanotechnol. 3 (2008) 101–105.
[51] W.S. Hummers, R.E. Offeman, J. Am. Chem. Soc. 80 (1958), 1339–1339.
[52] K. Kamegawa, K. Nishikubo, M. Kodama, Y. Adachi, H. Yoshida, Carbon 40 (2002) 1447–1455.
[53] G.W. Sun, J.T. Wang, X.J. Liu, D.H. Long, W.M. Qiao, L.C. Ling, J. Phys. Chem. C 114 (2010) 18745–18751.
[54] W. Sugimoto, H. Iwata, K. Yokoshima, Y. Murakami, Y. Takasu, J. Phys. Chem. B 109 (2005) 7330–7338.
[55] R.S. Hastak, P. Sivaraman, D.D. Potphode, K. Shashidhara, A.B. Samui, Electrochim. Acta 59 (2012) 296–303.